3D-Printed Ultra-Wideband In-Band Full-Duplex Antenna System with Grating Lobes Reduction

Hadi Hijazi, Marc Le Roy, Raafat Lababidi, Denis Le Jeune, André Pérennec

3D-Printed Ultra-Wideband In-Band Full-Duplex Antenna System With Grating Lobes Reduction

Hadi Hijazi[1,2*], Marc Le Roy[2], Raafat Lababidi[1], Denis Le Jeune[1], Andre Pérennec[2]
[1] ENSTA Bretagne and [2] Univ Brest, Lab-STICC, CNRS, UMR 6285, F-29200 Brest, France
*hadi.hijazi@ensta-bretagne.org

***Abstract*—This article presents an ultra-wideband in-band full-duplex antenna system based on a special 3D-printed Vivaldi array. To mitigate grating lobes inherent in such arrays, the single Vivaldi element size is reduced partially at its bottom and its body is exponentially tapered. In the array, this allows bringing the antennas closer together at their bottom parts, reducing the distance between the radiating slots, which translates to grating lobes reduction, especially at higher frequencies. The system can achieve, in simulation, a decade matching bandwidth from 2 to 20 GHz with more than 60 dB of self-interference cancellation and 12.8 dBi of average gain. The grating lobes remain at least 10 dB below the main lobe level throughout the matching bandwidth.**

Keywords—3D-printing, grating lobes reduction, in-band full-duplex, self-interference cancellation, ultra-wideband, Vivaldi antenna.

I. Introduction

In-band full-duplex (IBFD) technology permits two radio devices to communicate simultaneously using a single frequency, thus doubling the spectral resources in a frequency band. The main obstacle to achieve an IBFD communication are the self-interference (SI) signals which couple from the transmitter of one radio device to its own receiver. Thus, to establish such kind of communication, various self-interference cancellation (SIC) circuitry must be implemented at the different stages of the radio front-end: at the antenna, analog, and digital levels. IBFD gained popularity in the previous years [1] and lead to promising results in terms of the high levels of SIC obtained. Yet, most of these studies were based on narrowband systems, and there exist only few studies on wideband SIC [2-4]. Therefore, it is desirable to investigate this topic more. A wideband IBFD system can be used as a multi-standard radio for applications requiring high data-rate links or frequency reconfigurability, like radars, cognitive radios, or base stations.

Previously, we have designed an ultra-wideband IBFD antenna system that spans the frequency range from 4-40 GHz with at least 50 dB of self-interference cancellation [5]. The proposed system is configured as in Fig. 1(a), and it is composed of a 4-element PCB Vivaldi array and two baluns based on microstrip-slotline transitions. The wideband performance of both the antennas and baluns can be attributed to the wideband behavior of the microstrip-slotline transitions used in both devices. And those transitions were optimized for maximum bandwidth based on a previous study [6].

The four Vivaldi antennas in the array are placed vertically toward the direction of radiation, and then sequentially rotated around the center of the array as shown in Fig. 1(b). Thus, they form two pairs of orthogonally polarized antennas: one pair will be used to transmit while the other will be used to receive. Such antenna configuration is mandatory for proper system radiation and SIC. After that, each pair will be connected to an external balun which delivers, to the opposite antennas, two signals of equal amplitudes and inverted phases. The two radiated waves from the opposite antennas will cancel each other in the near-field region, where the other pair exists, and they will recombine constructively in the far-field region. The near-field cancellation and the orthogonal polarizations will ensure that the self-interference signals radiated by the transmit antennas will be cancelled by a significant amount (> 50 dB) before reaching the receive antennas.

But despite its wideband performance, the fabricated system suffered from three major drawbacks: (i) gain degradation due to high substrate losses, (ii) mechanical fragility due to low substrate thickness and the need for external support to hold the antennas, and (iii) presence of grating lobes in the radiation patterns, especially at higher frequencies, due to the excessive antenna separation in comparison to the corresponding wavelength.

In fact, all system components were built on a Rogers RO4003C substrate ($\varepsilon_r = 3.55, \tan\delta = 0.0027$) which proved to be extremely lossy in practice, especially at higher frequencies, leading to a significant drop in gain. Therefore, it is favorable to replace the used substrate with another one having lower loss tangent; for example, Rogers RT5880 ($\varepsilon_r = 2.2, \tan\delta = 0.0009$); or remove the substrate all together.

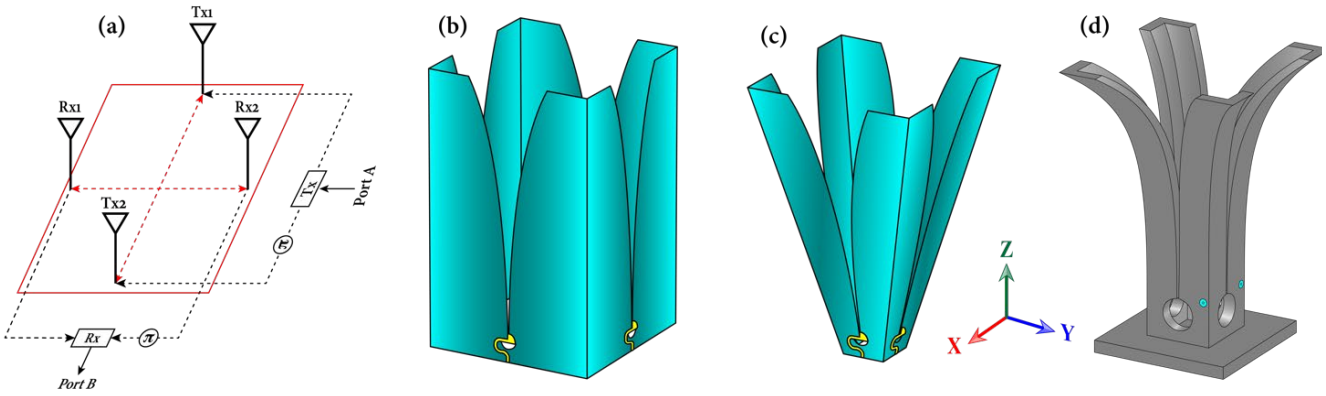

Fig. 1: (a) system configuration, (b) original PCB Vivaldi array design, (c) modified PCB array design with bottom size reduction, and (d) an exponentially tapered 3D-printed Vivaldi array with bottom size reduction.

Moreover, the wideband behavior of the microstrip-slotline transitions heavily relied on having a very low substrate thickness ($h = 203.2\ \mu m$), but this came at the expense of system's fragility and the need for an auxiliary support to hold the antennas and protect them from external forces. To overcome this, the thickness of the substrate can be increased but a portion of the bandwidth must be sacrificed.

Finally, it was noticed that there exist some grating lobes alongside the main lobe in one plane of the system radiation pattern. The grating lobes emerge when the separation distance between the two opposite antennas is higher than a half-wavelength at the corresponding frequency. This means that the grating lobes will be more significant at higher frequencies, and will multiply in number, considering that the separation distance between the antennas will be higher than a multiple of half-wavelength. Therefore, system size must be modified to reduce the grating lobes effect.

There are few degrees of freedom in PCB antennas that can be manipulated in order to enhance their performance, however, by shifting to 3D-printed antennas, one can manipulate antenna shape and metal thickness to modify the system's behavior. The final 3D-printed array is depicted in Fig. 1(d). In the next section, the mechanical design of the 3D-printed system will be discussed first, then a way to reduce grating lobes will be introduced after, and all will be followed by simulation results. Finally, the last section will conclude and point to future perspectives.

II. System Enhancement

A. Mechanical Enhancement

The main objective here is to build a sturdier system by shifting from PCB to thicker metallic sheets. And there exist a couple of industrial solutions that may accomplish this goal: either by metallized 3D-printing or by CNC milling. While both solutions have their merits, 3D-printing will be adopted here for availability and speed of fabrication. Though the motives to transition from PCB to 3D-printing are mainly mechanical, but there might also be some advantages for the electrical performance of the system:

i. The thickness of the printed parts can take almost any value, from less than a millimeter to several millimeters or even centimeters, unlike their PCB counterparts which are limited to the 0.1~3.2 mm range. By choosing a reasonable thickness for the antennas it can be made sure that the system is sufficiently rigid and can endure pressure from external forces.

ii. The rigidity of 3D-printing can permit to fabricate the entire Vivaldi array without the need for an external support to hold and align the antennas.

iii. The 3D-printing process can allow to shape the structure of the antennas in more liberal ways as opposed to the flat panel structure of PCBs. This property will be especially useful in the following section.

iv. No substrate is needed for the 3D-printing process and the antennas will be only surrounded by air, which eliminates dielectric losses and should enhance the gain.

The design process of the 3D-printed antennas should take into account two main variables. Firstly, the effect of metal thickness on the matching of the antenna and the surface current distribution along the antenna's flares. And secondly, the need to substitute the microstrip-slotline transitions of the PCB antennas with coax-slot transitions for the 3D-printed antennas. In this case, circular matching stubs are used in the 3D-printed model instead of the radial stubs used in the PCB, as it was evident from simulations that circular stubs provide better matching in the 3D-printing case while radial stubs are superior in the PCB case.

If a 50 Ω coaxial line is used to feed the antennas, then to avoid power reflections the slot impedance should match the coax impedance. In fact, the slot impedance is dependent upon two parameters: the slot width and the metal thickness. The metal thickness will be chosen to produce sufficiently rigid 3D-printed parts, while the slot width is only limited by the minimum dimensions that the 3D-printer can tolerate. Based on that, it was found that a slot width of 1 mm is acceptable by the 3D-printing process, and that the corresponding metal thickness should be 5.6 mm in order to obtain a 50 Ω slot.

It should be noted that the minimum width of the slot will determine the highest frequency of matching, while the radius of the matching stub will determine the lowest frequency of matching. The radius of the stub was set to 10 mm to obtain matching at 2 GHz, while it was found by simulation that a 1 mm slot limits the highest matching frequency to 25 GHz. And finally, the length of the exponential taper should be a wavelength at the lowest frequency and the width of the aperture should be a half-wavelength at that frequency to obtain good radiation [7]. This makes the total size of the antenna array in Fig. 1(d) $75 \times 75 \times 136$ mm^3.

B. Grating Lobes Reduction

Based on the fact that grating lobes originate from the excessive separation distance between the radiating antennas, particularly as it becomes greater than a half-wavelength, the obvious solution would be to bring the antennas closer together. However, because the antennas are configured in a box-like configuration where the transmit antennas are placed in-between the receive antennas, and vice versa, then the separation distance between one pair of antennas will be defined by the width of the other pair of orthogonal antennas. But since all antennas are identical, then the separation distance between the opposite antennas is conditioned by the width of the single element, which should be higher than λ/2 at the lowest frequency to ensure proper matching and radiation at the low-frequency end of the bandwidth.

A direct width curtailment will lead to a reduction in the electrical length of the antenna, and this in turn will lead to system performance deterioration at those low frequencies, which is undesirable in this case. The curtailed width can be compensated for by creating some corrugations in the sides of the antennas, which increases its electrical perimeter while keeping its size fixed. This permits the nonradiated surface currents to dissipate in the corrugations preventing them from reflecting to the input port. While this approach can preserve system matching, it cannot prevent the deterioration in its radiation at low frequencies. On the contrary, it might cause the corrugations to radiate to the sides of the antenna raising the levels of sidelobes.

Alternatively, an approach based on a partial width reduction can be considered a more acceptable solution. The rationale for this approach is based on three premises: (i) the grating lobes are much significant at higher frequencies where the separation distance becomes higher than multiples of a half-wavelength, (ii) the high-frequency radiation is emitted from the lower parts of the exponential taper while the low-

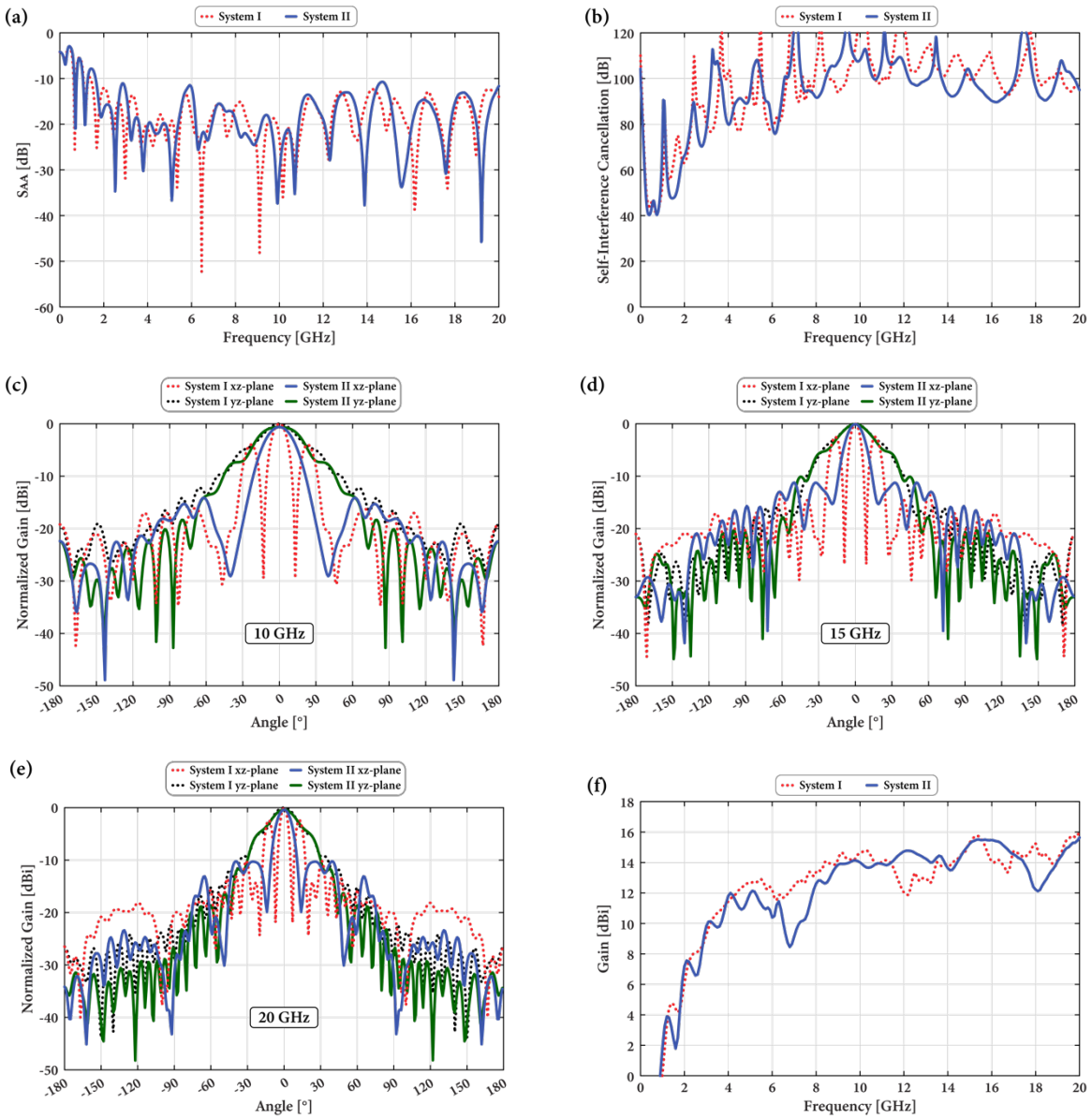

Fig. 2: simulated (a) system matching, (b) self-interference cancellation, (c), (d) and (e) radiation pattern plots at 10, 15 and 20 GHz respectively, and (f) system gain.

frequency radiation is emitted from the upper parts of the exponential taper, and (iii) the top part width is necessary for proper low-frequency radiation while the bottom part width is not critical for high-frequency radiation.

In light of the above, it can be inferred that by reducing the width of the bottom part of the single antenna, while keeping the same top part width, the radiation performance of the single element shall not be affected. This permits to bring the four antennas in the array closer together at their bottom parts, as shown in Fig. 1(c), while preserving the same separation at their top parts. Thus, in this case, it is necessary to tilt the antennas in the array forming a pyramid-like shape. The tilt angle (θ) with respect to the z-axis is given by:

$$\theta = sin^{-1}\left(\frac{W_t - W_b}{2L}\right) \qquad (1)$$

where W_t and W_b are the widths of the top and bottom parts of the antenna, respectively, and L is its length. It follows that the bottom parts of the exponential tapers, which are responsible for high-frequency radiation, are now closer than before, and this should mitigate the grating lobes at higher frequencies. And on the other hand, the low-frequency radiation will be insignificantly affected by this approach.

The same approach was applied to the 3D-printed array in Fig. 1(d), however with a slight change. In fact, the body of the 3D-printed antennas were tapered exponentially giving the array a lily-flower-like shape, contrary to the PCB antennas which can be only tapered linearly. Exponential tapering of the antennas' bodies allows the lower parts of the antennas to be brought even closer towards the center of the array, as opposed to the fixed separation in the PCB case, which should boost the grating lobes reduction even more.

Finally, though this step alone is not sufficient to eliminate entirely the grating lobes, it remains a better arrangement than the initial design. Nevertheless, there should be a concern whether the tilt in the antennas would cause some problems in the array's performance, considering that the radiation of the single element is not emitted along the broadside direction, but

rather along a slightly tilted path. This issue will be discussed and analyzed next.

C. Simulation Results

Simulations were carried out using CST Microwave Studio in which the antennas were modeled as perfect electric conductors (PECs). Similarly, the metallic parts of the coaxial cables were also modeled as PECs, while the dielectric part of the coax was modeled as Teflon ($\varepsilon_r = 2.1, \tan\delta = 0.0002$). Moreover, two microstrip-slotline baluns operating in the frequency range from 2 to 20 GHz were also designed and simulated based on [6]. The results of the simulation are depicted in Fig. 2, and they compare two different systems: 'System I' is a 3D-printed design where the antenna size is uniform and there is no size reduction; this is similar to the PCB design in Fig. 1(b); and 'System II' is the 3D-printed lily-shaped design in Fig. 1(d) where the antenna size is reduced at the bottom and its body is exponentially tapered.

Beginning with system matching in Fig. 2(a), it seems that both systems exhibit similar matching figures, where both systems are well matched over a decade bandwidth from 2 to 20 GHz. Equally, it can be said that both systems exhibit similar self-interreference cancellation performance, where in Fig 2(b), the level of cancellation remains higher than 60 dB and it maintains an average value of 100 dB. Note that these values are idealistic and are expected to be lower in practice, as it was observed in our previous study [5], since they ignore the impact of fabrication intolerances, and the imbalances between the balun's outputs on the array's performance.

In addition to the above, Fig. 2(c), 2(d), and 2(e) depict some radiation pattern plots at 10, 15, and 20 GHz, respectively. It should be noted here that the plots correspond to the transmit antennas which are situated along the x-axis, in Fig. 1(d), and orthogonal to the xz-plane. The plotted radiation patterns indicate that the yz-plane cuts are quite similar for both systems, though it can be said, in general, that System II exhibits lower sidelobe levels. Also, it is evident that grating lobes are only present in the xz-plane, and that their levels are much lower for System II. Moreover, other sidelobes in general are lower in System II. In fact, the obtained grating lobe reduction is about 9.5, 8.7, and 7.4 dB at 10, 15, and 20 GHz, respectively. And this confirms the validity of the grating lobe reduction approach proposed here. At last, those figures show that the radiation at all frequencies is directed along the broadside, which means that tilting the antennas does not cause a tilt in the direction of the array's radiation.

Finally, the gain plots in Fig. 2(f) show that the average gain of System I in the matching bandwidth is about 13.2 dBi, while it is 12.8 dBi for System II. For both plots, there are severe gain dips at some frequencies; for example, around 6~7 GHz; however, they seem stronger for System II and occurring at slightly different frequencies. Our simulations revealed that, for both systems, there is a strong direct coupling between the opposite antennas at those frequencies. This direct coupling does not hinder the self-interference cancellation performance of the system, but it surely deteriorates its gain. And although we were not able to exactly pinpoint the root cause of this problem, yet our simulations indicate that there is a high correlation between this phenomenon and the size of the matching stubs and the proximity of the two opposite stubs. More precisely, if the size of the stub is reduced, or if the separation between the opposite stubs is increased, then the gain dips become less significant or occur outside the matching bandwidth.

III. Conclusion

In summary, this paper presented an ultra-wideband IBFD antenna system based on a 3D-printed Vivaldi array. To mitigate grating lobes inherent in such array, the Vivaldi antennas' size was reduced partially at the bottom and the bodies of the antennas were exponentially tapered. In the array, this allows bringing the antennas closer together at their bottom parts, reducing the distance between the radiating slots, which translates to grating lobes reduction especially at higher frequencies. The system can achieve, in simulation, a decade matching bandwidth from 2 to 20 GHz with more than 60 dB of self-interference cancellation and 12.8 dBi of average gain. The grating lobes remain at least 10 dB less than the main lobe level throughout the matching bandwidth.

The proposed grating lobes reduction approach appears not to deteriorate system matching and self-interference cancellation performance, but it deepens some gain dips occurring at some frequencies. The gain dips are accompanied by a strong power coupling between the opposite antennas, which is thought to be caused by the size of the matching stubs and their proximity. Several solutions are being investigated for this problem, including but not limited to manipulating the shape and position of the matching stubs, inserting absorbing materials between the antennas, creating corrugations to confine or discharge the direct power coupling. And finally, a prototype of the proposed array will be fabricated and measured once the above-mentioned problem is solved.

References

[1] K. Kolodziej, B. Perry,and J. Herd, "In-band full-duplex technology: Techniques and systems survey." IEEE Transactions on Microwave Theory and Techniques, 2019, vol. 67, no. 7, pp. 3025-3041.

[2] E. A. Etellisi, "Wideband Monostatic Co-Channel Simultaneous Transmit and Receive (C-STAR) Antenna and Array Systems." PhD diss., University of Colorado at Boulder, 2018.

[3] P. V. Prasannakumar, "Wideband bi-static and monostatic STAR antenna systems." PhD diss., University of Colorado at Boulder, 2019.

[4] H. Hijazi. "Systèmes d'antennes Ultra-Large-Bande pour Applications In-Band Full-Duplex." PhD diss., Université de Bretagne Occidentale, Brest; École Nationale Supérieure de Techniques Avancées Bretagne, 2021.

[5] H. Hijazi, M. Le Roy, R. Lababidi, D. Le Jeune, and A. Pérennec, "Ultra‐Wideband Antenna System for In‐Band Full‐Duplex Applications." IET Microwaves, Antennas & Propagation 15, no. 15, pp. 1853-1865, 2021.

[6] H. Hijazi, M. Le Roy, R. Lababidi, D. Le Jeune, and A. Pérennec, "4-40 GHz In-Phase/180 Out-of-Phase Power Dividers with Enhanced Isolation." In 2020 14th European Conference on Antennas and Propagation (EuCAP), pp. 1-5. IEEE, 2020.

[7] C. A. Balanis, "Antenna Theory: Analysis and Design". John wiley & sons, 2015.